International Journal of Nanomedicine

Dovepress
Taylor & Francis Group

Open Access Full Text Article

ORIGINAL RESEARCH

Cutaneous Evaluation of Fe_3O_4 Nanoparticles: An Assessment Based on 2D and 3D Human Epidermis Models Under Standard and UV Conditions

Claudia Geanina Watz[1–4], Elena-Alina Moacă[4,5], Andreea Cioca[6], Lenuța Maria Șuta[7], Lavinia Krauss Maldea[2], Ioana Zinuca Magyari-Pavel[8,9], Mirela Nicolov[2,3], Ioan-Ovidiu Sîrbu[10,11], Felicia Loghin[12], Cristina A Dehelean[4,5]

[1]Doctoral School, "Victor Babes" University of Medicine and Pharmacy, Timisoara, 300041, Romania; [2]Department of Pharmaceutical Physics, Faculty of Pharmacy, "Victor Babes" University of Medicine and Pharmacy, Timisoara, 300041, Romania; [3]Center for Drug Data Analysis, Cheminformatics and the Internet of Medical Things, "Victor Babes" University of Medicine and Pharmacy, Timisoara, 300041, Romania; [4]Research Center for Pharmaco-Toxicological Evaluation, "Victor Babes" University of Medicine and Pharmacy, Timisoara, 300041, Romania; [5]Department of Toxicology and Drug Industry, Faculty of Pharmacy, "Victor Babes" University of Medicine and Pharmacy, Timisoara, 300041, Romania; [6]Department of Pathology "Regina Maria" Health Network, Timisoara, 300645, Romania; [7]Pharmaceutical Technology, Faculty of Pharmacy, "Victor Babes" University of Medicine and Pharmacy, Timisoara, 300041, Romania; [8]Department of Pharmacognosy-Phytotherapy, "Victor Babes" University of Medicine and Pharmacy Timisoara, Timisoara, 300041, Romania; [9]Research and Processing Center for Medicinal and Aromatic Plants, "Victor Babeș" University of Medicine and Pharmacy, Timisoara, 300041, Romania; [10]Department of Biochemistry, Faculty of Medicine, "Victor Babes" University of Medicine and Pharmacy Timisoara, Timisoara, 300041, Romania; [11]Complex Network Science Center, "Victor Babes" University of Medicine and Pharmacy Timisoara, Timisoara, 300041, Romania; [12]Department of Toxicology, Faculty of Pharmacy, "Iuliu Hatieganu" University of Medicine and Pharmacy of Cluj-Napoca, Cluj-Napoca, 400012, Romania

Correspondence: Elena-Alina Moacă, "Victor Babes" University of Medicine and Pharmacy, Timisoara, 300041, Romania, Tel +40745762600, Email alina.moaca@umft.ro

Purpose: The high-speed development of nanotechnology industry has fueled a plethora of engineered nanoparticles (NPs) and NP-based consumer products, further leading to massive and uncontrolled human exposure. In this regard, the researches addressing the safety assessment of NPs should be re-approached from the perspective of test parameters variety, closely simulating daily life scenarios. Therefore, the present study adopts complex in vitro models to establish the safety profile of Fe_3O_4 NPs, by using 2D and 3D human epidermis models under both standard and UV exposure conditions.

Methods: Advanced 3D human reconstructed epidermal tissues and two different monolayers of immortalized human cells (keratinocytes and fibroblasts), using series of in vitro assays were employed in the current study to evaluate multiple biological responses, as follows: i) divers protocols (skin irritation, phototoxicity assay); ii) different conditions (± UV exposure) and iii) a wide variety of quantification methods, such as: MTT, NR and LDH colorimetric tests – performed to evaluate the viability of the cells/microtissues, respectively, the cytotoxicity of the test compounds. In addition, IL-1α ELISA assay was used to quantify the inflammatory activity induced by the test samples, while immunocytochemistry analysis through fluorescent microscopy was employed to provide insightful information regarding the possible mechanism of action of test samples.

Results: The two test samples (S_1 and S_2) induced a higher cell viability decrease on immortalized human keratinocytes (HaCaT) compared to human fibroblasts (1BR3), while 3D-epidermis microtissues showed similar viabilities when treated with both samples under standard conditions (-UV rays) – for both type of evaluation protocols: skin irritation and phototoxicity. However, UV irradiation of 3D-microtissues pre-exposed to test samples led to different results between the two test samples, revealing that S_2 sample induced a significant impairment of human epidermis viability, whereas S_1 sample elicited an activity similar to the one recorded under standard conditions (-UV).

Conclusion: The present results indicate significant differences in toxicity between the two in vitro models under UV conditions, highlighting the importance of model selection and exposure parameters in assessing NP safety. Thus, our findings suggest that Fe_3O_4 NPs may pose some risks under specific environmental conditions, within the limitations of the experimental setup, and further research is needed to refine safety guidelines.

Keywords: cytotoxicity, magnetite NPs, 3D-microtissue, UV, HaCaT, 1BR3

Received: 22 December 2024
Accepted: 11 March 2025
Published: 20 March 2025

Introduction

Human exposure to engineered nanoparticles (NPs) has increased considerably in recent years due to myriad of NPs applications in the commercial products, though investigations concerning their potential toxicological impact is still in progress.[1] NPs uptake into the human body is mainly achieved through three entry routes: i) oral ingestion; ii) inhalation and iii) skin penetration.[2] Even though several studies discuss aspects regarding oral ingestion[2–5] and inhalation[6] of NPs, the literature is scarce of data concerning the dermal penetration of NPs and the resulting health outcome.[7] However, according to the comprehensive study published by Vance and collaborators, the assessment of 770 nanotechnology-enabled products along with their possible exposure pathways declared the skin as the main exposure organ responsible for NPs entry. This fact may be caused by a plethora of products that are especially manufactured to be in contact with the skin or the hair.[1] Also, a large number of NPs-based consumer products are personal care or cosmetic items and are therefore targeted for topical application.[8]

An important role among NPs is played by magnetite NPs (Fe_3O_4 NPs). Their applications in the cosmetics industry being beneficial due to the detoxifying and antioxidant properties, as they provide skin protection by capturing and neutralizing free radicals and reducing oxidative stress, thereby helping to prevent, to some extent, premature skin aging.[9] Furthermore, Fe_3O_4 NPs can be used for the transport and gradual release of active substances, enabling more effective penetration into the skin while also optimizing their distribution through external stimuli (magnetic fields).[10] Although NPs offer numerous advantages, they also bring challenges related to scalability, stability, costs, and toxicity, thus their safety and toxicity profiles remain subjects of intense debate.

Due to their small size, large surface area, and positive charge, NPs interact with the biological microenvironment, potentially exhibiting dose-dependent toxicity and the risk of increasing the concentration of active substances that reach the circulatory system. Numerous recent studies have focused on deepening the understanding of interactions between NPs and skin, taking in consideration the possible nanotoxicological impact of the NP-based test compounds, especially when undergoing a long-term contact[11] or UV exposure.[12]

Regarding the biocompatibility and chemical stability of Fe_3O_4 NPs, several studies emphasize the importance of biological testing to prevent toxic reactions or adverse effects that pose health risks in both biomedical and cosmetic applications.[13,14] However, even though UV irradiation is widely applied to these NPs for various proposes, such as photocatalyzing systems for biological applications[15–17] or for the synthesis of magnetically stabile aqueous nano-formulations (ie Fe_3O_4-chitosan NPs),[18] thus endorsing the stability of Fe_3O_4 NPs under UV irradiation and the possible lack of reactive compounds generation under these conditions, investigation of magnetite NPs as potential skin irritant compounds still represents a topic of interest for various domains, such as: cosmetics,[19] textile industry,[20] tattoos,[21] nanotoxicology management[22] and wastewater treatment,[17] especially since metal and metal oxide NPs are described as the most utilized kind of NPs on the market and the skin considered to be the main entry route.[1]

Nevertheless, in addition to the NPs physico-chemical behaviour to UV rays, another important factor plays a key role in the safety screening of the NPs at the skin level: UV irradiation of cutaneous tissue, which can induce a significant negative impact on the skin that weakens the skin's protective barrier, by causing oxidative damage and affecting cellular DNA in the form of thymine dimers, that may further lead to skin inflammation and suppress immunity,[23] resulting in premature aging (UVA rays) and even in increased risk of skin cancer, including melanoma (UVB rays).[24] Also, the US Government Accountability Office (GAO) revealed that significant side effects can be induced by NPs presence in sunscreens that can penetrate damaged skin, endorsing the importance of biological testing and safety assurance.[25] Thus, taking into consideration all the above-mentioned aspects, regardless of the type of NP, biological screening must not lose sight of the effects that the skin could manifest after being presensitized by NP-skin contact, following subsequent exposure to UV irradiation. An aspect that may closely simulate possible real-life scenario. Therefore, to obtain a comprehensive screening profile, biological evaluations of NP-induced effects at the skin level should be performed both on healthy models (standard conditions) and on UV-irradiated models. Yet, to the best of our knowledge, no study has investigated the potential toxicological effects of Fe_3O_4 NPs pre-sensitized skin cells following UV irradiation, a scenario that may occur in real life under certain circumstances.

All data presented above regarding: i) the highly increasing exposure of humans to nano-based products and ii) the UV impact on the skin level, amplifies the implementation of a comprehensive pre-marketing testing, especially when

referring to topical exposure, as already mentioned, the cutaneous tissue is considered the most targeted site for nano-enabled formulations.[1,8]

However, strict regulations on the use of animals for in vivo testing of cosmetics or personal care products make the in vivo testing strategy to seem unapproachable. This fact may have led to discrepancy between the need for studies evaluating the commercial NP-based products on skin and the actual number of studies that approach this issue; as since 2009, the use of animals for evaluation of acute toxicity of cosmetics has been forbidden and is governed by the Seventh Amendment (2003/15/EC) of the Cosmetic Directive (76/768/EEC). Moreover, beginning with March 2013, the requirements broaden to evaluations regarding chronic (repeated exposure) toxicity, carcinogenicity and toxicokinetic of cosmetic products and cosmetic ingredients. The aim of these regulations is to ensure animal welfare by developing complex alternative in vitro methods based on human tissue models that can efficiently reveal the human behavior following the testing of cosmetic products.[26–28] In response to these regulations, the European Commission has acknowledged the European Centre for the Validation of Alternative Methods (ECVAM) for the responsibility of leading and supervising all the steps necessary for the validation of in vitro alternative methods. Thus, ECVAM-validated tests aim to replace in vivo animal testing.[29] Therefore, MatTek company has developed an ECVAM-validated assay (OECD TG 439) for evaluation of skin irritation potential of test products (liquids and solids) on human reconstructed epidermis model – EpiDerm^{TM} along with another protocol for phototoxicity assessment of the samples.[30]

Taking into consideration the need for biological screening of metal NPs by implementing validated and standardized in vitro alternative methods, the present study was designed to offer insight information related to the security profile of two different Fe_3O_4 NPs on human skin for both standard (-UV) and UV-treated in vitro models, along with the impact risks converging from it. Therefore, the assessment of the possible skin irritation potential and the phototoxic impact of two Fe_3O_4 NPs samples (S_1 and S_2) on 3D human reconstructed epidermal models under standard parameters and UV irradiation was employed. In addition, the cytotoxic potential of the samples (S_1 and S_2) on two immortalized human cell lines from skin origin (keratinocytes – HaCaT and fibroblasts – 1BR3 cells), was also assessed under standard and UV parameters, obtaining different data depending on the 2D in vitro cell model employed. Thus, the present study is intended to represent a pioneering research in the safety assessment field of NPs and should be considered as a model, especially for traditional-simplistic experimental designs that should be re-approached from the perspective of the variety of test parameters that should closely simulate daily life scenarios.

Materials and Methods

Magnetite (Fe_3O_4) NPs Test Samples (S_1 and S_2)

Method

Both Fe_3O_4 NPs tested in the present study were synthesized through combustion method using the $Fe(NO_3)3{\cdot}9H_2O$ as an oxidizing agent and $C_6H_8O_7{\cdot}H_2O$ as a fuel.[31] Both recipes were designed to obtain 0.03 mol of Fe_3O_4 NPs, with some differences in the synthesis process; therefore, their physicochemical properties are slightly different.

Experimental Setup

Firstly, to obtain sample (S_1), a stoichiometric amount of reactants was used, while for the second sample (S_2), a double stoichiometric amount was used, with a purity correction to $Fe(NO_3)3{\cdot}9H_2O$ of 98% applied in addition (Figure 1). The experimental methodology for both samples was described in detail in our previously published articles, as follows: Moaca et colab[32] describes the synthesis process for sample S_1 and reference[33] describes the synthesis of sample S_2.

Data Analysis

The first sample (S_1) presents a diameter between 8.22 and 23.0 nm and the magnetic properties translate into a value of 53 emu/g, as described in a previous published article;[32] while, the second sample (S_2) displays a diameter ranging in size from 4.26 to 13.1 nm and saturation magnetization of 46.26 emu/g, as presented in another recently published article.[33]

Nevertheless, a more detailed comparison in terms of physico-chemical features of the two test samples (S_1 and S_2) can be consulted in Table 1.

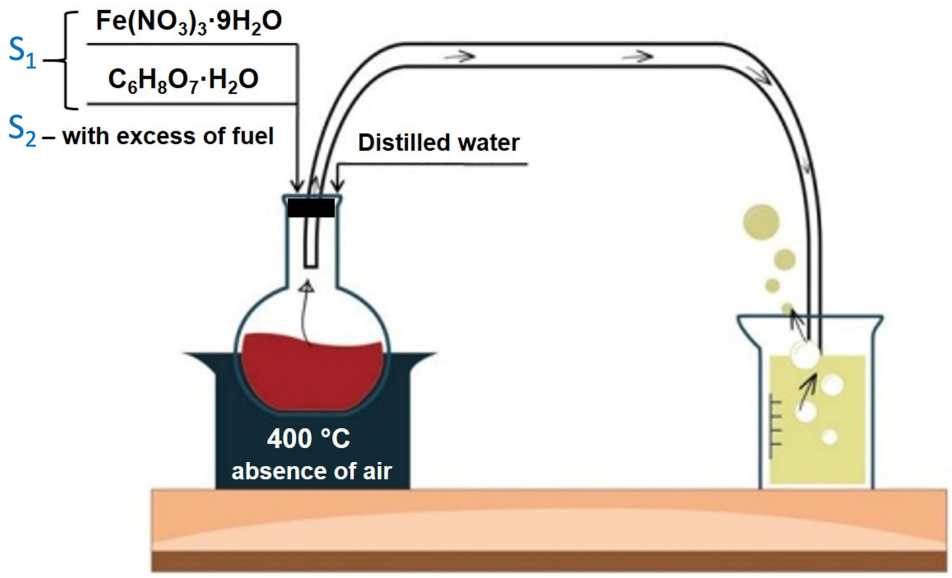

Figure 1 Schematic representation of Fe_3O_4 NPs synthesis through combustion method.

Cell Lines and Cell Culture Conditions

Materials

The 2D cell lines used in the current study were immortalized human keratinocytes (HaCaT – catalog no. 300493, CLS Cell Lines Service GmbH) and human skin fibroblasts (1BR3 – catalog no. 90011801, European Collection of Authenticated Cell Cultures). The sterile media used for cell proliferation were: i) Dulbecco's modified Eagle medium with high glucose of 4.5 g/L (DMEM) and ii) Eagle's minimum essential medium (EMEM), both media being acquired from American Type Cell Collection (ATCC), while the supplements – foetal bovine serum (FBS), trypsin/EDTA and penicillin/streptomycin mixture were purchased from Sigma Aldrich (Munich, Germany).

Experimental Setup

HaCaT cells were cultured in DMEM media enriched with 10% FCS, while 1BR3 cells were cultured in EMEM supplemented with 15% FBS. Both cell lines were supplemented with 1% antibiotic mixture of penicillin/streptomycin solution and cultured under sterile conditions and further maintained in humidified atmosphere at 37°C and 5% CO_2 using a Steri-Cycle i160 incubator (Thermo Fisher Scientific, Inc., Waltham, MA, USA).

Data Analysis

Viability Assessment on 2D Cell Cultures ± UV Exposure by Means of Neutral Red (NR) Assay

This method evaluates the percentage of viable cells by taking advantage of the lysosomes capacity to incorporate the neutral red dye through active transport, thus under acidified extracted conditions only the viable cells will be able to release the incorporated stain. In the present study, Neutral Red Assay Kit – cell viability/cytotoxicity ab234039 (Abcam, Cambridge, United Kingdom) was used, according to the manufacturer's protocol.

Table 1 Several Features of S_1 and S_2 Samples Obtained Through Combustion Method

Sample	Phase Composition	D_{XRD} [nm]	D_{TEM} [nm]	Ms [emu/g]
S_1	Fe_3O_4	18	8.22–23.0	53
S_2	Fe_3O_4	9	4.26–13.1	46.26

In brief, the cells (HaCaT and 1BR3) were cultured in 96-well plates to an initial density of 10^4 cells/well. When the confluence reached 80%, the old media was removed, and the cells were exposed for 18h to two different samples of Fe_3O_4 NPs (S_1 and S_2) using concentrations of 25, 50, 100, 150, 200 µg/mL. Afterwards, the medium was replaced with 1× PBS and the cells were maintained in 50 µL/well 1× PBS for UVA irradiation (a procedure that avoids the possible formation of phototoxic compounds released by the cell culture medium under UV conditions). UV irradiation was realized by employing a wavelength of 365 nm and a cumulative dose of 300 mJ/cm^2 (0.3 J/cm^2) which might simulate a real-life scenario.[34] The irradiation procedure was performed at room temperature – RT by means of Biospectra system (Vilber Lourmat, France).

In the same time, another plate was maintained under standard conditions (-UV), at RT, in a dark chamber. When the UV irradiation was finished, both types of plates (containing UV irradiated cells and no irradiated cells) were washed with 1× PBS, stained with 150 µL/well of 1 x NR solution and incubated for 2h. Afterwards, the cells were washed again and for the final step 150 µL/well of 1× solubilization solution was added. The optical density of the released dye was measured at 540 nm wavelength and further used to quantify the rate of viable cells, by applying the following formula:

$$Cell\ viability\ (\%) = \frac{O.D.sample}{O.D.negative\ control\ (cells\ treated\ with\ medium)} \times 100$$

Nuclear and Lysosome Staining of HaCaT Cell Line Under Standard and UV Conditions

To observe the detailed changes that may occur inside the cells when treated with two different Fe_3O_4 NPs (S_1 and S_2) under specific conditions (standard and UV treatment), a double staining was performed for two important cellular compartments: lysosomes and cell nuclei. In this regard, lysosomal staining kit – green fluorescence – cytopainter ab112136 (Abcam, Cambridge, United Kingdom) was used for lysosomal staining, while Hoechst 33342 reagent was used for cell nuclei counterstaining by employing a working solution of 1:2000 dilution in 1× PBS.

The exposure parameters (±UV) of cell cultures and the stimulation treatment (18h) with S_1 and S_2 samples were identical to the ones described for the cell viability assessment.

EpiDerm™ Model

Materials

Two reconstructed three-dimensional (3D) human epidermis model kits (EPI-200-SIT and EPI-200-PHO, Lot 30838 and Lot 30890), containing multiple viable human keratinocytes layers and a functional stratum corneum, were purchased from MatTek Life Science Company (Bratislava, Slovak Republic). The 3D-epidermis model is an ECVAM-validated skin model to assess skin irritation and represents an assay governed by OECD TG 439.

Experimental Setup

EpiDerm™ Standard Operation Procedures (SOP) – A Phototoxicity Test and Irritancy Assessment

To perform both the in vitro skin irritation and phototoxicity tests, the epidermis inserts were removed from agarose, wiped and transferred to 6-well plates containing 0.9 mL/well of assay medium for 1h. Afterwards, the medium from the wells was removed and 0.9 mL/well of fresh medium was added followed by incubation overnight in humidified atmosphere with 5% CO_2 at 37°C. The next day, all inserts were treated for 18h with two different Fe_3O_4 NPs (S_1 and S_2), following the moisturizing of the tissue surface with DPBS to improve contact of the epidermis surface with both Fe_3O_4 NPs samples (S_1 and S_2). Duplicate samples of epidermis inserts were used for each test compound.

(a) After stimulation, the test irritation protocol was employed as follows: each epidermis insert was repeatedly rinsed with DPBS to remove the test samples and were further prepared for the MTT viability assay, as described in another subsection. Meanwhile, the medium left in the wells was further used for LDH and IL-1α quantification.

(b) For phototoxicity protocol the inserts were transferred after 18h into a new 6-well plate pre-filled with 900 µL/well of DPBS. Afterwards, half of the inserts were exposed to UVA irradiation by employing a wavelength of 365 nm and a cumulative dose of 6 J/cm^2, using the Biospectra system (Vilber Lourmat, France). The UVA exposure was performed at room temperature – RT.

The irradiation intensity was in good agreement with the manufacturer's SOP and Kandarova's group.[30] Also, the protocol respected the OECD test guideline for testing of chemicals on reconstructed human epidermis for phototoxicity assessment.

Meanwhile, the UVA-free plates were maintained in the dark at RT. When the irradiation protocol was completed, all the inserts were carefully washed with DPBS and the inserts were placed into another 6-well plate pre-filled with 1h-acclimatized assay medium (0.9 mL/well) and further incubated overnight.

Data Analysis

Viability Assay of EpiDerm™ Model for Irritancy and Phototoxicity Protocols via MTT Test

To evaluate the viability of epidermis inserts, the 3-(4,5-Dimethylthiazol-2-yl)-2,5-diphenyltetrazolium bromide (MTT) assay was performed. In brief, 300 µL of 1mg/mL MTT solution in DMEM was added into each well of a 24-well plate before the microtissues were transferred. The 24-well plate containing the epidermis inserts was incubated for 3h and afterwards the insoluble formazan products were extracted overnight at 4°C in 2mL isopropanol. In the next day, 4 samples of 200 µL aliquots of each extracted formazan solution were transferred to a 96-well plate, and the optical density (OD) of the samples was determined at 570 nm using a microplate reader (xMark™ Microplate, Bio-Rad Laboratories, Hercules, CA, USA).

Afterwards, the following formula[35] was used to evaluate the irritancy potential of test samples:

$$Microtissue\ viability\ (\%) = \frac{O.D.sample}{O.D.negative\ control\ (inserts\ treated\ with\ DPBS)} \times 100$$

Cytotoxicity of EpiDerm™ Model Using Lactate Dehydrogenase (LDH) Release Test

The LDH release assay was employed to evaluate the cytotoxic potential of S1 and S2 samples under standard conditions and UV irradiation. In this regard, after the stimulation protocol of epidermis models was accomplished, the medium surrounding the inserts was harvested and used for LDH quantification, as described in detail in another recently published article.[36] For this method, the Pierce LDH Cytotoxicity Assay Kit (ThermoFisher Scientific, No 88954) was employed.

Quantification of Inflammatory Markers of EpiDerm™ by Assessing Interleukin 1 Alpha (IL-1α) via ELISA Method

To assess the IL-1α release of the stimulated 3D-reconstructed human epidermis models into the culture media, an enzyme-linked immunosorbent assay (Human IL-1 alpha ELISA kit, Invitrogen, ThermoFisher Scientific, Cat No BMS243-2) was performed, according to the manufacturer protocol, by quantifying the anti-human IL-1α antibody absorbed on the bottom of the microwells that reacts with the human IL-1α released by the microtissues (into the medium) after exposure to S_1 and S_2 ± UV. Further, a biotin conjugated anti-human IL-1α antibody interacts with the human IL-1α bound by the first antibody (free biotin-conjugated antibody is removed during a washing step). In the following step, addition of streptavidin-HRP reacts with the biotin-conjugated anti-human IL-1α antibody (free Streptavidin-HRP is removed during a washing step), afterwards the substrate solution reactive containing HRP is added, and a blue colored product reaction is obtained. The intensity of the blue color is proportional to the concentration of human IL-1α released into the media. The optical density is determined at 450 nm wavelength using a microplate reader (xMark™ Microplate Spectrophotometer, Bio-Rad Laboratories, Inc., Hercules, CA, USA). Human IL-1α amount (pg/mL) was quantified based on a standard curve generated from seven human IL-1α standard dilutions ($R^2 = 0.9983$).

Histopathological Assessment of 3D Reconstructed Human Epidermis Models

For histopathological analysis, the 3D models were fixed in 10% buffered formalin for 48 h and afterwards were embedded in paraffin. Four µm-thick sections were cut using a Leica Rotary Microtome (Leica Biosystems Nussloch GmbH, Nussloch, Germany) and mounted on glass slides, deparaffinized in xylene and rehydrated. Finally, the samples were stained with the conventional Hematoxylin & Eosin (H&E). Image acquisition and analysis were performed using a Nikon Eclipse E 600 microscope (Nikon Microscopes/Instruments Division, Vienna, Austria).

Statistical Analysis

GraphPad Prism 9 version 9.3.01 (GraphPad Software, San Diego, CA, USA) was used for graphical representation and statistical analysis. Data are presented as mean values ± standard deviation (SD). One-way ANOVA was performed to obtain the statistical differences, followed by Dunnett's post-test. Statistically significant differences between negative control group (-UV) *versus* exposed groups were labelled with asterisks, as follows: *p < 0.1; **p < 0.01; ***p < 0.001; ****p < 0.0001.

Results

Cell Viability Assessment of the 2D Keratinocytes and Fibroblasts Cultures Under Standard and UV Conditions via NR Assay

As shown in Figure 2, both cell lines (HaCaT and 1BR3 cells) presented good cell viability (above 91.76% for HaCaT and above 92.3% for 1BR3), after exposure to five different concentrations (25, 50, 100, 150, 200 µg/mL) of test samples (S_1 and S_2), under standard conditions (-UV). However, the results showed that both cell lines manifested a slight cell viability decrease after exposure to UV radiations, observing that HaCaT cell population was more affected, compared to 1BR3 cells, as following: HaCaT control cells + UV presented a viability of 93.1%, whereas under the same exposure conditions (+UV radiation), 1BR3 control cells showed a viability of 96.4%. However, both cell lines respected the same trendline, showing a slight decrease of cell viability while increasing the concentrations of both Fe_3O_4 samples (S_1 and S_2). Nevertheless, the most significant impact on cell viability was recorded when the cells were exposed to UV radiations following treatment with S_2 sample; in this situation HaCaT cells elicited a viability rate of 80.9%, while 1BR3 cells presented a viability of 89.92%.

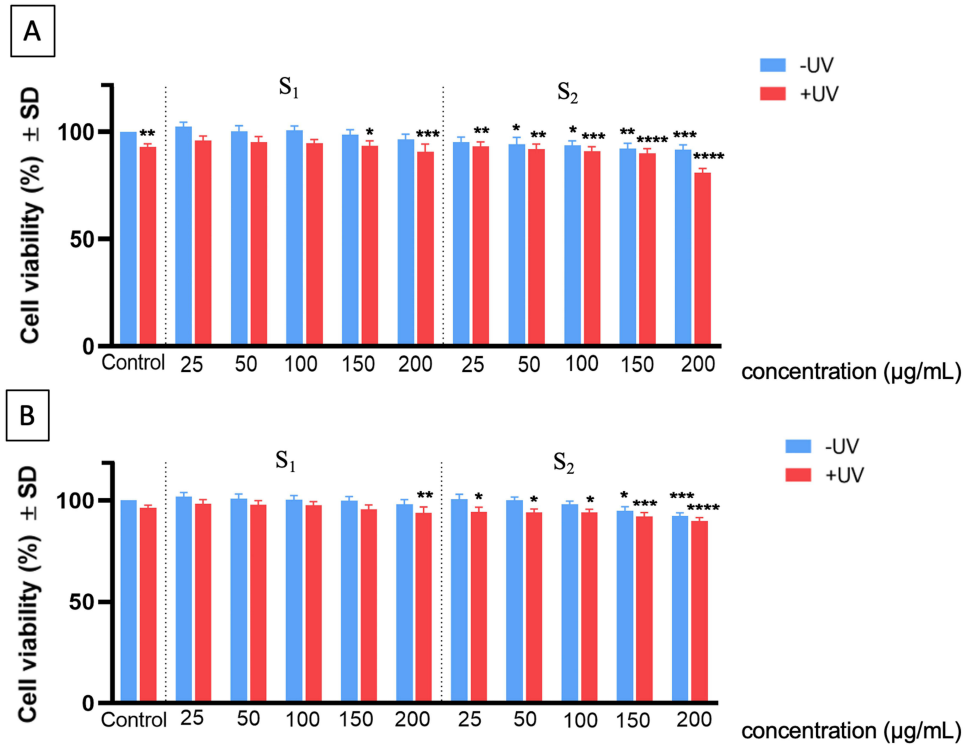

Figure 2 The effect induced by Fe_3O_4 test samples (S_1 and S_2) on: (**A**) human keratinocytes HaCaT and (**B**) human fibroblasts - 1BR3 at 18 h post-stimulation under standard and UV conditions, employing the NR assay. Results are presented as cell viability percentage (%) normalized to negative control cells (cells treated with medium, under standard conditions). The data represent the mean values ± standard deviation (SD) of three independent experiments. One-way ANOVA analysis was applied to determine the statistical differences followed by Dunnett post-test (*p < 0.1; **p < 0.01; ***p < 0.001; ****p < 0.0001 *versus* control cells -UV, considered as negative control).

https://doi.org/10.2147/IJN.S513423

Nuclear and Lysosome Staining of 2D Human Keratinocytes (HaCaT Monolayer) Under Standard and UV Conditions

To better understand the cytotoxic effect induced by NP samples, the 2D cell culture that underwent the most significant impairment after exposure to S_1 and S_2 samples (represented by HaCaT cell line, as revealed through NR assay) was treated with the highest test concentration (200 µg/mL), under standard and UV conditions, in order to assess the impact of the samples on the nuclear and lysosome compartments of HaCaT cell culture, by employing fluorescence microscopy visualization, as presented in Figures 3 and 4.

As shown in Figure 3, HaCaT control cells (±UV) present good nuclear and lysosomal morphology, the cell nuclei showing no signs of chromatin condensation, nuclear membrane blebbing or DNA fragmentation, whereas the lysosomal compartment presents normal distribution and localization close to the nucleus, a specific feature for interphase of cell division. However, as depicted in the enlarged pictures through red arrows, a high number of lysosomes present accumulation of the S_1 sample, under both parameters (-UV/+UV), but no significant alteration of the lysosomal compartment was observed. Also, HaCaT cell nuclei elicit normal morphological features after 18h post-exposure to S_1, thus revealing that the mechanism of action responsible for S_1 activity on HaCaT cells is closely related to a lysosome-mediated pathway.

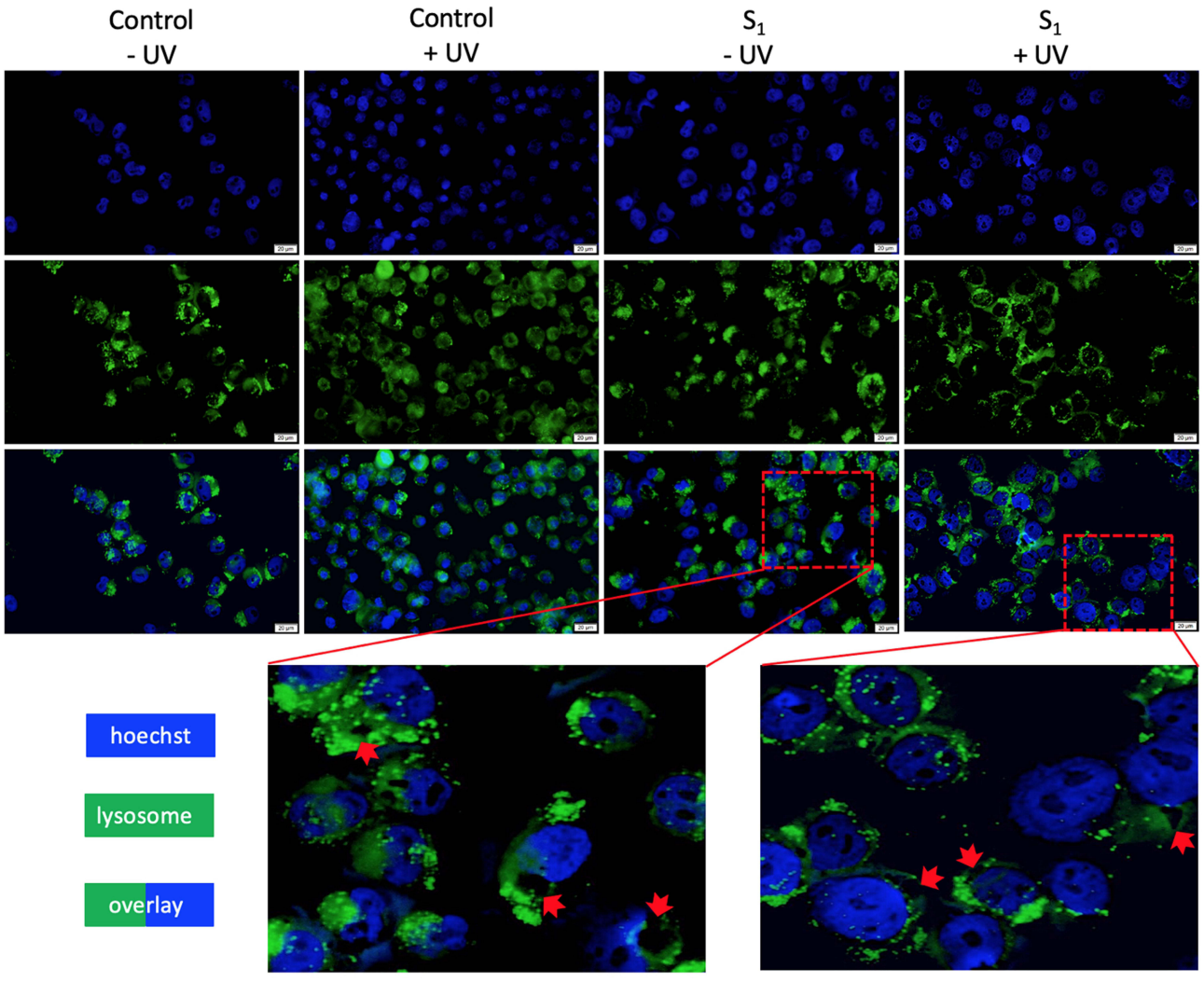

Figure 3 Immortalized human keratinocytes (HaCaT) monolayer visualized by fluorescence microscopy at 18h post-exposure to S_1 (concentration of 200 µg/mL), under standard (-UV) and UV parameters. Nuclear and lysosome staining was presented both ways: i) separated (hoechst and lysosome) and combined (overlay). Red arrows present the accumulation of Fe_3O_4 NPs, preponderantly in the lysosome compartment. Control cells -UV were considered as negative control. Scale bar represents 20 µm.

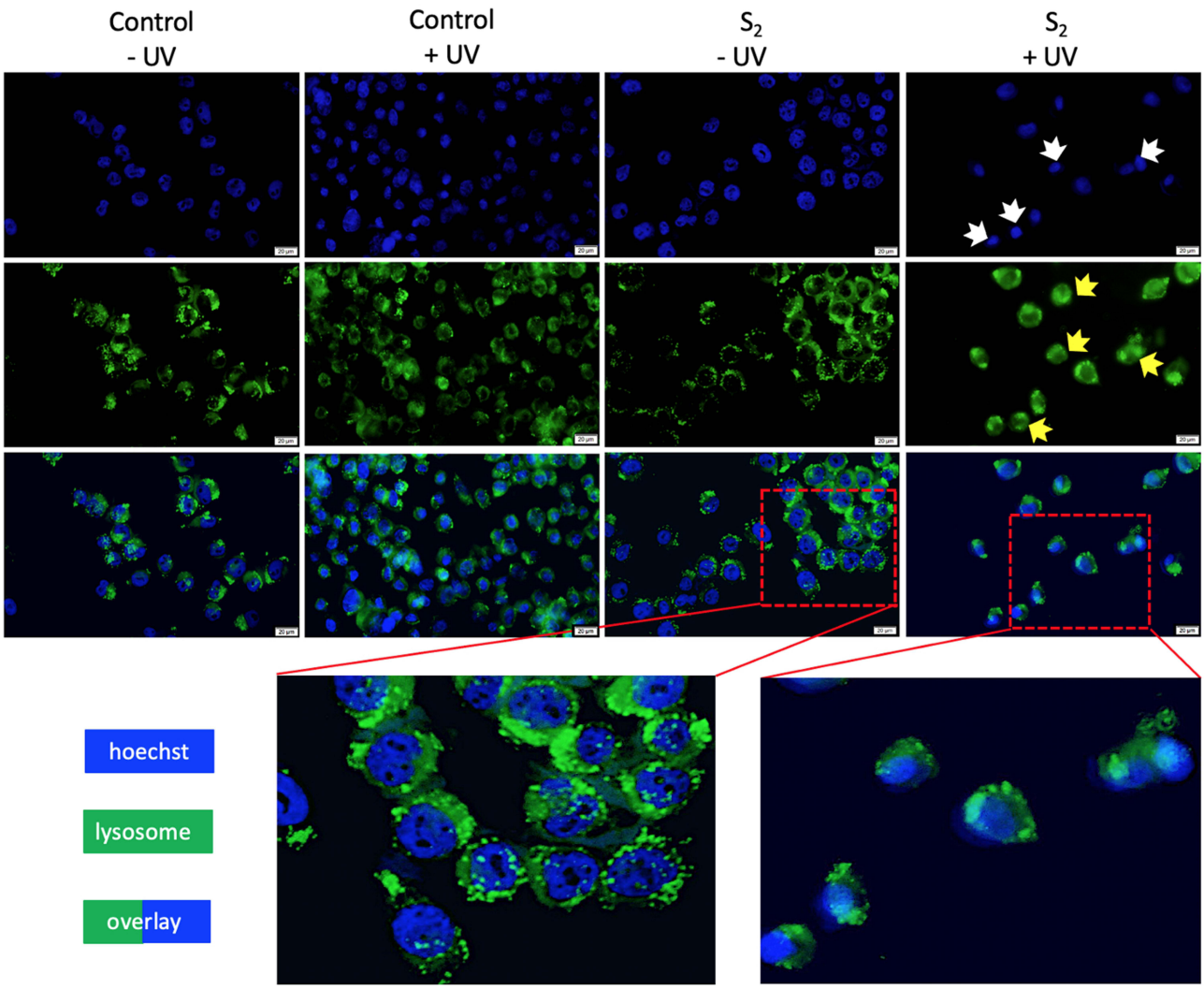

Figure 4 Immortalized human keratinocytes (HaCaT) monolayer visualized by fluorescence microscopy at 18h post-exposure to S_2 test sample, under standard (-UV) and UV parameters. Nuclear and lysosome staining was presented both ways: i) separated (hoechst and lysosome) and combined (overlay). Cell nuclei alterations are indicated by white arrows and lysosomal impairment is marked by the yellow arrows. Control cells -UV were considered as negative control. Scale bar represents 20 µm.

The double staining of nuclear and lysosome compartments of the 2D human keratinocyte model revealed normal morphological aspects – a good chromatin distribution within cell nuclei and normal lysosomal features for both control cells (no exposure to UV and UV-treated cells). Also, HaCaT cells treated with S_2 sample for 18h, under standard conditions (-UV) presented normal nuclear elements with only few lysosomal alteration signs.

However, the immortalized human keratinocytes treated with S_2 (200 µg/mL) under UV conditions were significantly affected regarding both: i) the nuclear characteristics (observing a condensation of the chromatin – indicated by the white arrows) and ii) the lysosome features (observing their diffuse distribution with an increase in volume, which is pointed out by the yellow arrows), as presented in Figure 4.

Nevertheless, the images did not reveal Fe_3O_4 accumulation within the lysosomal compartment of HaCaT cell culture when treated with S_2 sample (200 µg/mL) for 18h, under both standard (-UV) and UV-treated cells (+UV), in contrast to the accumulation phenomenon observed when the HaCaT culture was exposed to S_1 sample employing the same experimental conditions (ie concentration, time treatment interval and ±UV rays).

https://doi.org/10.2147/IJN.S513423

Irritation and Phototoxicity (± UV) Evaluation of EpiDerm™ Inserts via MTT, LDH and IL-1α Assays

As presented in Figure 5, none of the tested Fe_3O_4 NPs (S_1 and S_2) showed a significant irritating potential on the reconstructed human epidermis model; S_1 and S_2 samples induced a cell viability of 89.87 ± 2.8% and 85.20 ± 1.06%, respectively. Also, the results are sustained by the quantification of the LDH amount released by epidermis inserts in the culture medium, revealing that the test samples did not induce a cytotoxic effect on the reconstructed human skin model – S_1 induced a cytotoxicity percentage of 4.07 ± 1.09%, while S_2 manifested a cytotoxicity rate of 6.95 ± 1.02%, following an interval of 18h stimulation time.

The phototoxicity protocol employed under standard conditions (-UV) revealed similar viability percentages of the 3D-epidermis models as the ones obtained within the irritancy test. However, when exposed to UV irradiation (total dose of 6 J/cm^2), epidermis inserts treated with test samples (S_1 and S_2) elicited lower viability rates of 75.84 ± 0.15% and 69.2 ± 0.16%, representing a decrease of more than 10% for both samples when compared to the viability rates obtained under standard conditions (-UV).

The cytotoxicity assessment of epidermis microtissues revealed no important LDH leakage into the medium, yet the highest level of LDH was noticed under UV radiation, obtaining cytotoxic rates of 4.58 ± 0.11% for S_1 and 9.03 ± 0.31% for S_2.

Even if in the 2D models, S_2 sample induced only a maximum rate of 20% reduction in cell viability at concentrations of 200 µg/mL (+UV), in the 3D models, the same concentration caused a 31% reduction in viability of the microtissues. A discrepancy that highlights the increased sensitivity of 3D reconstructed human epidermis to nanoparticle toxicity, especially when 3D models are further exposed to UV stress.

When referring to the possible inflammatory activity of the sample-treated microtissues (Table 2), no important release of the interleukin 1 alpha (IL-1α) was quantified into the culture media, recording concentrations of IL-1α close to

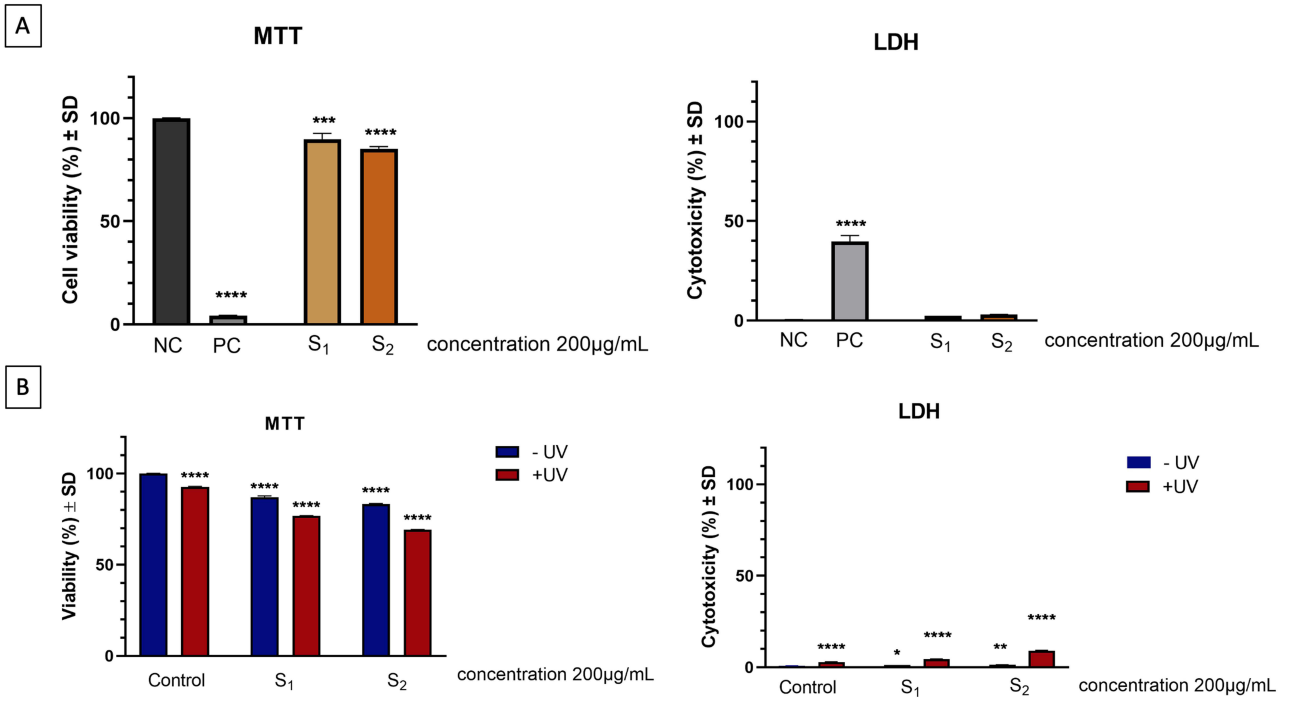

Figure 5 Irritation (**A**) and phototoxicity data (**B**) of 3D reconstructed human epidermis after exposure to 200 µg/mL of S_1 and S_2 for a period of 18h. Results are presented as viability percentage (%) normalized to negative control = NC (microtissues treated with medium, under standard conditions -UV). The data represent the mean values ± standard deviation (SD) of three independent experiments. Positive control (PC) is represented by SDS 1%. One-way ANOVA analysis was applied to determine the statistical differences followed by Dunnett post-test (*p < 0.1; **p < 0.01; ***p < 0.001; ****p < 0.0001 *versus* control cells -UV, considered as NC).

Table 2 Inflammatory Marker (IL-1α) Release of 3D Reconstructed Human Epidermis After Exposure to 200 µg/mL of S_1 and S_2 for a Period of 18h via ELISA Method

Irritancy Assessment	***PC** SDS 1%***	***NC* DPBS***	***S_1***	***S_2***
IL-1α (pg/mL)	19.73 ± 0.52	2.25 ± 0.03	2.53 ± 0.03	3.1 ± 0.04
Phototoxicity evaluation	***Conditions***	***NC****	***S_1***	***S_2***
IL-1α (pg/mL)	-UV +UV	1.71 ± 0.01 8.6 ± 0.06	10.5 ± 0.04 16.07 ± 0.07	12.56 ± 0.14 20.98 ± 0.23

Notes: *NC = negative control; **PC = positive control.

the ones released by the negative control microtissue, when the irritancy evaluation protocol was employed. However, the inflammatory marker (IL-1α) augmented into the media 18h post-exposure of epidermis inserts to S_1 and S_2 samples, when the phototoxicity protocol was employed, as follows: the amount of IL-1α increased when 3D-microtissues were further exposed to UV irradiation – from 10.5 ± 0.04 pg/mL (-UV) to 16.07 ± 0.07 pg/mL (+UV) after treatment with S_1, while for the 3D microtissue exposed to S_2 the amount of IL-1α grew from 12.56 ± 0.14 pg/mL (-UV) to 20.98 ± 0.23 pg/mL (+UV), revealing an important inflammatory marker release, especially for the UV-treated 3D human reconstructed epidermis models.

Histopathological Assessment by H&E Staining

The skin samples from the control group had a normal histological structure (Figure 6A), while the control group exposed to UV radiations showed a slight increase of the keratin layer (hyperkeratosis) and moderate accumulation of epidermal

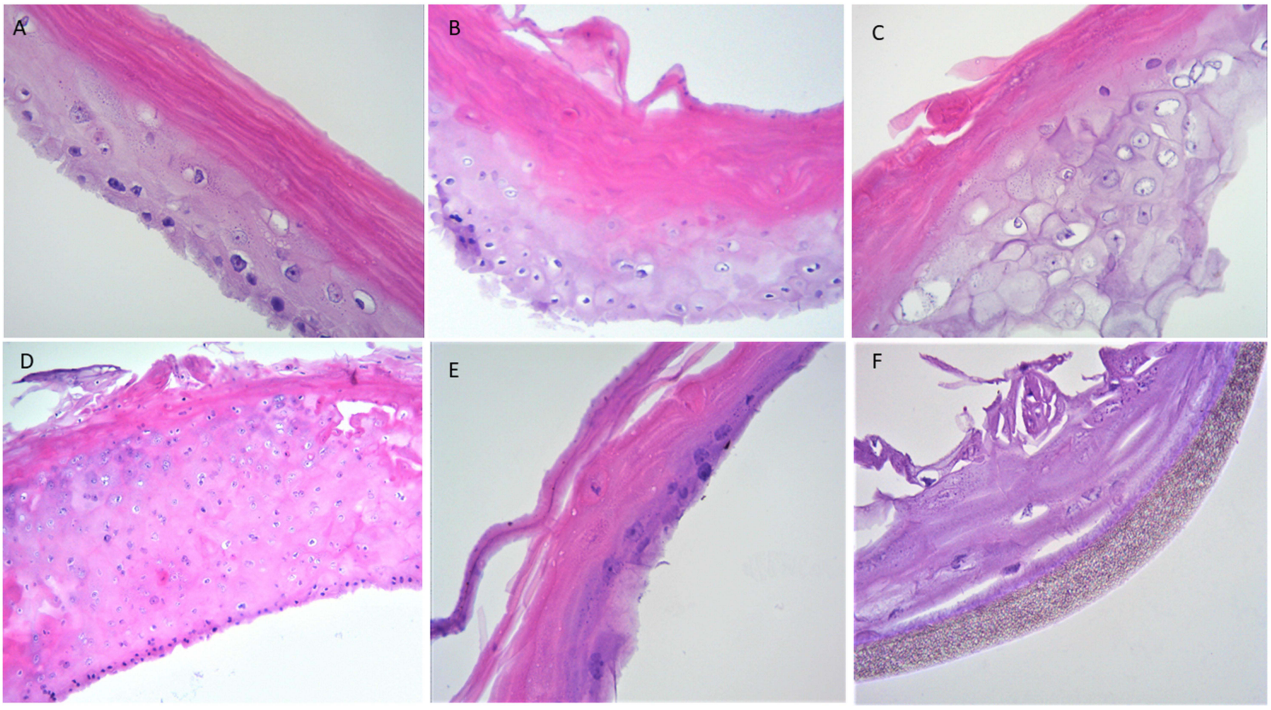

Figure 6 Histopathological examination of the 3D skin models by H&E staining. Section from the untreated control microtissue, considered as negative control x40 (**A**); control group exposed to UV showing epidermal hyperplasia and hyperkeratosis, x10 (**B**). Group treated with S_1 depicted signs of epidermal hyperplasia and hyperkeratosis, x40 (**C**), and superficial erosion following UV exposure, x10 (**D**). Topical application of S_2 revealed erosion of the epithelium with less viable cells, x40 (**E**); with more significant erosion aspects recorded for the UV-irradiated microtissue with S_2, x40 (**F**).

https://doi.org/10.2147/IJN.S513423

keratinocytes, namely epidermal hyperplasia (Figure 6B). Topical application of S_1 depicted a thick epidermis, with many proliferated keratinocytes, some of them showing reactive changes as binucleation, cell vacuolization and visible nucleoli (Figure 6C). Moreover, the surface of the epidermis showed several superficial signs of erosion, an aspect that was more evident when the 3D-microtissue was exposed to UV radiations (Figure 6D). Compared with the group exposed to S_1, the one treated with S_2 was more affected and showed evident erosions of the epidermis, with less viable keratinocytes (Figure 6E). A more significant effect was also observed when the group was exposed to UV radiations (Figure 6F).

Discussion

When referring to the physicochemical features of the test samples (S_1 and S_2), the reaction stoichiometry is a critical factor influencing the synthesis of magnetic iron oxide NPs (MIONPs), particularly in determining the phase, size, and magnetic properties of the resultant samples. The stoichiometric balance between iron and oxygen during combustion directly affects the formation of different iron oxide phases, such as magnetite (Fe_3O_4) and maghemite (γ-Fe_2O_3), which exhibit distinct magnetic characteristics and applications in various fields, including biomedicine and catalysis.[37–39] Moreover, the use of iron(II) and iron(III) sources can lead to different outcomes, affecting the resultant particle size and morphology. However, the present study used the same iron source(III) for Fe_3O_4 NP generation, but different stoichiometric reports between oxidizer and fuel, obtaining the same phase composition (ie Fe_3O_4), perhaps due to the work condition (absence of air), yet the physicochemical features of the samples obtained were distinct (see Table 1).

Nevertheless, it has been shown that precise control over the stoichiometry can yield nanoparticles with desired magnetic properties, as variations in the iron-to-oxygen ratio can lead to changes in the oxidation state of iron, which is crucial for the magnetic behavior of the nanoparticles.[40,41] The formation of iron oxide nanoparticles through combustion often results in a complex interplay of oxidation and reduction reactions, where the stoichiometric balance can dictate the efficiency of the synthesis process and the properties of the final product,[42,43] the reason why the present study implemented an alternative to the current methods to obtain the magnetite nanoparticles, which requires low amounts of energy as it consists of a single-step process, has a short duration and is also environmentally friendly. Thus, a simple and facile technique for obtaining the Fe_3O_4 NPs was developed by our group using no air atmosphere, by bubbling the gases resulting from the combustion process into a vessel with distilled water (see Figure 1).

Stoichiometry refers to the quantitative relationship between reactants and products in a chemical reaction, it is often expressed in terms of the equivalence ratio, which is the ratio of the actual fuel-to-oxidizer ratio to the stoichiometric fuel-to-oxidizer ratio. Variations in this ratio can significantly influence the combustion characteristics. One can observe that the granule size depends on the reaction stoichiometry since a combustion reaction does not occur for any molar fuel/oxidizing agent ratio. In addition, when the fuel was added in excess, the saturation magnetization was slightly lower, as well as the crystallite size determined by X-ray diffraction (see Table 1). Probably, this is due to the organic residues resulting from fuel combustion. Our findings are in agreement with the literature, which states that the morphology and phase composition of combustion products can also be affected by stoichiometry. Variations in stoichiometry can lead to changes in particle morphology and combustion temperatures, which in turn influence the overall efficiency of the synthesis process.[44,45] This is particularly relevant in self-propagating high-temperature synthesis, where the stoichiometric balance between reactants can dictate the extent of combustion and the characteristics of the resulting materials.[46,47]

Therefore, the influence of reaction stoichiometry on the combustion synthesis of iron oxide magnetic nanoparticles is complex, involving the careful selection of precursors, control of the fuel-to-oxidizer ratio, and optimization of synthesis conditions. These factors collectively determine the phase, size, and magnetic properties of the nanoparticles, which are critical for their applications in medicine.[37–39,48]

On the other hand, when referring to the NPs applications in the biomedical field and particularly on the skin level, the most studies have been closely focused on the enhancement performance of products, including: superior UV protection, increasing hydration power, supporting skin regeneration and pigmentation uniformity, boosting encapsulation efficiency, enhancing dermal penetration and active substance release, as well as improving physical stability.[25,49] However, the toxicological screening of nano-enabled products should also be a constant concern and should especially include the recently developed validated alternative methods, such as 3D in vitro reconstructed human epidermal models designed for the safety assessment of skin care products, as these methods may represent the future in pre-marketing testing.

Advances in 3D skin models have become more efficient compared to traditional 2D models and they also provide an ethical alternative to toxicological testing on animals. 2D cultures have numerous limitations: lack of cell-to-cell and cell-to-extracellular matrix interactions, loss of morphological, functional, and metabolic specificity, and inability to simulate heterogeneous diseases, thus greatly reducing the accuracy of toxicity assessment.[50] The advantages of the 2D model for in vitro evaluations remain the low cost and simplicity (accessibility) of testing. These models fail to accurately reproduce the in vivo microenvironment for skin and offer limited perspectives on the physiological reactions of the body to external stimulus, limiting their value in complex toxicological and biological studies.[51,52] However, 3D models replicate more accurately the structure of human skin, providing a more precise assessment of skin toxicity, irritation, and sensitization.[51] Furthermore, 3D bioprinting enables the integration of multiple cell types, such as adipocytes, fibroblasts, and keratinocytes, creating a full layer of skin composed of the epidermis, dermis, and hypodermis. Complex structures (blood vessels) can also be replicated through bioprinting, though this often involves significant technical challenges (high costs, complex technical validation and interpretation).[53]

3D human reconstructed epidermal models were already successfully employed to assess the toxicological profile of several nano-enabled formulations at skin level, such as proniosomal gel,[54] Ag NPs[55] or a wide variety of metallic NPs (iron, aluminum oxide, titanium oxide and silver).[56] However, to the best of our knowledge no study has investigated the impact of iron oxide NPs at skin level using UV-irradiated 3D human functional epidermis models.

Thereby, the present study includes 3D in vitro microtissues (designed by MatTek Life Science Company, Bratislava, Slovak Republic) to evaluate the safety profile in terms of irritation potential and phototoxic impact of two physico-chemically different Fe_3O_4 NPs (S_1 and S_2) on human epidermis. The data obtained (Figure 5) revealed a similar impact of S_1 and S_2 samples on the 3D microtissues when both types of assessment methods (irritancy and phototoxicity) were employed, by obtaining similar viability percentages of the 3D-reconstructed human epidermis when no UV radiation was applied, as follows: i) S1 sample induced a viability of 89.87 ± 2.8% under the irritancy protocol, while a viability rate of 87.06 ± 0.69% was recorded after the phototoxicity protocol employment; ii) S_2 sample presented a similar pattern, inducing a viability of 85.20 ± 1.06% under the irritancy protocol and a viability rate of 83.32 ± 0.38% when the phototoxicity method was performed. However, different effects depending on the test sample (S_1 versus S_2) were recorded when the phototoxicity assessment was performed using UV irradiated models, the viability rates decreasing by more than 10% when compared to the standard condition (-UV) data, as follows: S_1 sample induced a viability of 87.06 ± 0.69% under standard condition (-UV), while the viability percentage recorded for the UV-treated microtissues was 76.84 ± 0.15%; S_2 sample induced a viability of 83.32 ± 0.38% under standard parameters (-UV) and a viability rate of 69.2 ± 0.16% when the 3D-reconstructed human epidermis was further exposed to UV rays.

Nevertheless, according to the study published by Kandarova and collaborators,[31] a sample is not associated with an irritant potential if the cell viability of the inserts employed for the skin irritation protocol is above 50%, therefore none of the test sample (S_1 and S_2) should be labelled as an irritancy-inducing compound.

Yet, the histopathological examination (Figure 6) revealed important erosion features of the UV-irradiated micro-tissues treated with S_2, while the 3D-reconstructed epidermis treated with S_1 showed only signs of hyperkeratosis and hyperplasia (under the same UV conditions), an aspect that was also observed for the control microtissue exposed to UV rays. Thus, even though the S_2 sample should not be considered an irritant compound, a recommendation should be issued regarding a biofriendly coating of the NPs surface, that may further tailor its colloidal stability[57] and possibly the biomedical acceptance. Several approaches that may enhance the biological acceptance of the NPs are based on: i) polymer coatings: ie silica layers[58,59] or chitosan coated NPs,[60] surfactant-enabled stabilization[61] or ii) direct incorporation of NPs in different nano-platforms such as: magnetoliposomes[62,63] or solid-lipid nanoparticles (SLN).[64]

The present study also assessed the test samples (S_1 and S_2) on two different human skin cells: immortalized human keratinocytes (HaCaT) and human fibroblasts (1BR3) quantifying the cell viability percentages by means of the neutral red (NR) colorimetric assay, a method that evaluates the ability of the viable cells to assimilate the NR reagent within their lysosomal compartment, that further leads to the viability rate quantification by comparing the NR lysosomal uptake rate of the xenobiotic-treated cells to the NR lysosomal uptake percentage of the control cells.[57,65]

Moreover, it has already long been established that NPs toxicity is strongly linked with lysosomes activity,[66,67] thus NR assay could be considered a well-founded technique due to its capacity to evaluate the integrity of the lysosomal

compartment and should provide insight data regarding the basic pathways involved in the present Fe_3O_4 NPs test samples (S_1 and S_2) cytotoxic activity.

The relatively low UV cumulative dosage of 0.3J/cm^2 employed for the irradiation of the 2D cell cultures post-exposure to Fe_3O_4 NPs was selected as it could simultaneously meet two different criteria: it may simulate more closely a real-life scenario, being also correlated with several transformations at keratinocytes level, such as activation of ErbB2.[34]

The results obtained in the present study via the NR assay revealed that under the same exposure conditions (concentration, time exposure and ± UV stress) the human keratinocytes cell line (HaCaT 2D model) expressed a lower cell viability rate, compared to the human fibroblast monolayers (1BR3 cell culture), obtaining a concentration-dependent viability decrease pattern, as follows: i) for the HaCaT model the viability rates ranged between 102.45% and 91.76% (when the cells were not exposed to UV rays) and between 95.92% and 80.9% (post-UV exposure); ii) the 1BR3 in vitro model elicited viabilities of 101.81% and 92.3% when the cells were not irradiated, while the viability rates recorded for the same cell line after UV exposure were between 98.26% and 89.92%, for the same test concentrations, between 25 and 200 µg/mL. Thus, the results obtained through the NR assay revealed that the potential cytotoxic activity of the test samples (S_1 and S_2) may be related to the lysosomal compartment impairment translated to the NR uptake capacity of the cell-treated lysosomes.

Nevertheless, the literature presents several pathways involved in Fe_3O_4 NPs-induced apoptosis/necrosis, such as: reactive oxygen species (ROS) production, lysosomal impairment and mitochondrial function alteration of BAX/BCL-2 ratio.[32] Other studies even discuss the relation played by surface coatings in lysosomal uptake rate, which may further affect the degradation of the NPs, thus influencing ROS or other pathways involved in iron oxide cellular mechanism of action.[68,69] Therefore, considering this information, for a more insight into the mechanism of action of the test samples, both the nuclear staining and lysosomal counterstaining of the HaCaT cells treated with test samples under standard (-UV) and UV conditions were performed, and the acquired images were analyzed by means of fluorescent microscopy, as presented in detail in Figures 3 and 4. Nevertheless, the method endorsed our assumption, revealing different degrees of sample accumulation at the lysosome level and cytotoxic effects related to this phenomenon; thus, HaCaT control cells under the two exposure conditions (-UV/+UV) exhibited no important signs of cells nuclei alteration or lysosome impairment features, the lysosomal compartment presenting standard distribution and a normal localization in close proximity to the nucleus, a specific feature for interphase of cell division.[70] However, S_1 sample presented a high accumulation rate at lysosome level of HaCaT cells, with no important cytotoxic activity (see Figure 3), while S_2 sample, even though did not present high accumulation rate at the lysosome level, induced important cellular alterations of the HaCaT monolayer at both the nuclear and lysosomal levels, only under UV exposure conditions.

As already mentioned before in this study, even though S_2 sample did not induce important alteration under standard conditions, the UV-treated epidermis models revealed a different cytotoxic potential of S_2 sample. This constitutes an aspect that should draw attention to the increased sensitivity of 3D models to nanoparticle toxicity, when exposed to UV stress. In addition, the phenomenon observed herein highlights the importance of safety screening of materials using advanced 3D in vitro models and simulating different conditions that may occur in real-life scenarios, such as when the cutaneous tissue come in contact with Fe_3O_4 NPs followed by a relatively low UVA exposure. Also, this research underscores the fact that studies evaluating material safety should no longer be limited to classical monolayer cell cultures that may bypass some biological outcomes, possible due to the limited skin microenvironment reproduction that fails to offer accurate physiological feedbacks to external stimulus.[50,52,55]

Nevertheless, both samples (S_1 and S_2) can be considered safe for human skin exposure under standard conditions, when the following parameters are employed: contact time of 18h and concentration up to 200 µg/mL. In addition, S1 sample induced similar results under UV exposure conditions as well, results that are in good agreement with other recently published studies that sustain the innocuous effect of MIONPs at human skin level, as follows: Eric F. Bernstein et al[71] reports the inclusion of Fe_3O_4 NPs in sunscreen formulations as an effective and safe method not only for protection against UVA and UVB radiation but also against high-energy visible (HEV) blue light while also contributing to shade formation that makes them more cosmetically appealing. Similar results were obtained by Elbrolesy, A and collab.,[72] when magnetite (the colored oxide that can protect the skin from visible light, being biodegradable and non-

toxic once it enters the human body) was combined with ZnO nanoparticles. Thus, the resulting sunscreens were considered non-toxic, biocompatible, and to possess an extended radiation-blocking capacity (UVA and visible light). Another study, which evaluated the impact of magnetite on human dermal fibroblasts using 72 hours cell stimulation time, revealed no major changes of cell viability, even when this long time interval was employed.[73] Also, knowing that Fe_3O_4 NPs are magnetic NPs and could be used in different nanoplatforms as tools for magnetic stimuli-enabled nanoplatforms, our group has recently investigated the impact of magnetic field for a period of approximately 30 min on skin derived-cell cultures (HaCaT and A431), revealing that up to a frequency of 312.4 kHz and amplitude of 370 G, no important cytotoxic effects are caused.[74,75]

The present study would like to underline the fact that a direct comparison of the results obtained by employing 2D in vitro models and 3D human reconstructed microtissues may constitute a limitation of the current study due to the incongruence of the two in vitro models and also due to different UV cumulative dosage used for the irradiation of the in vitro models (monolayers versus 3D microtissues), which may not be transposed exactly from one model (2D) to the other one (3D).

Conclusion

To provide a complex safety profile of test compounds, it is absolutely necessary to employ advanced screening methods and varied experimental parameters (different assays, several concentrations and different exposure conditions of in vitro models ± UV irradiation). The present research being the first one that evaluated the potential toxicological effects developed by Fe_3O_4 NPs using in vitro human 2D and 3D skin models under UV conditions. Therefore, increased attention should be paid to each type of compound when assessing its security profile, since, as revealed in the present research, usual external conditions (such as UV rays) or small changes of the physico-chemical characteristics of test samples can lead to quite different biological results, even if the synthesis method of the samples is identical. In the particular case evaluated in the current research, S_1 sample did not induce an important viability impairment of human epidermis models, showing also a lysosomal-dependent mechanism of action, while S_2 sample did not present high lysosomal uptake rate within human keratinocytes, showing detrimental activity on reconstructed human epidermis, especially when the 3D-microtissues were exposed to UV irradiation. Thus, the present findings revealed that within the limitations of the study regarding the incongruence of the two in vitro models and UV irradiation dosage, some Fe_3O_4 NPs may give rise to undesirable effects under specific environmental conditions (UV stress) and further investigations are requested to sharpen the safety guidelines.

Acknowledgments

This research was funded by the Advanced Research Contract – Young Researchers: No. 1686 of 26.01.2024, from "Victor Babeș" University of Medicine and Pharmacy, Timișoara (Project manager: Claudia G. Watz). The authors would like to acknowledge "Victor Babeș" University of Medicine and Pharmacy Timisoara for the financial support in covering the costs of publication for the present research paper.

Disclosure

The authors report no conflicts of interest in this work.

References

1. Vance ME, Kuiken T, Vejerano EP, et al. Nanotechnology in the real world: redeveloping the nanomaterial consumer products inventory. *Beilstein J Nanotechnol*. 2015;6(1):1769–1780. doi:10.3762/bjnano.6.181
2. Fröhlich E, Roblegg E. Oral uptake of nanoparticles: human relevance and the role of in vitro systems. *Arch Toxicol*. 2016;90(10):2297–2314. doi:10.1007/s00204-016-1765-0
3. Stalder T, Zaiter T, El-basset W, et al. Interaction and toxicity of ingested nanoparticles on the intestinal barrier. *Toxicology*. 2022;481:153353. doi:10.1016/j.tox.2022.153353
4. McCracken C, Dutta PK, Waldman WJ. Critical assessment of toxicological effects of ingested nanoparticles. *Environ Sci Nano*. 2016;3(2):256–282.
5. Askri D, Ouni S, Galai S, et al. Nanoparticles in foods? A multiscale physiopathological investigation of iron oxide nanoparticle effects on rats after an acute oral exposure: trace element biodistribution and cognitive capacities. *Food and Chemical Toxicology*. 2019;127:173–181. doi:10.1016/j.fct.2019.03.006

6. Kononenko V, Warheit DB, Drobne D. Grouping of poorly soluble low (Cyto)toxic particles: example with 15 selected nanoparticles and a549 human lung cells. *Nanomaterials*. 2019;9(5):704. doi:10.3390/nano9050704
7. Brouwer DH, Spaan S, Roff M, et al. Occupational dermal exposure to nanoparticles and nano-enabled products: part 2, exploration of exposure processes and methods of assessment. *Int J Hyg Environ Health*. 2016;219(6):503–512. doi:10.1016/j.ijheh.2016.05.003
8. Yoshioka Y, Kuroda E, Hirai T, et al. Allergic responses induced by the immunomodulatory effects of nanomaterials upon skin exposure. *Front Immunol*. 2017;8:169. doi:10.3389/fimmu.2017.00169
9. Abdulsada FM, Hussein NN, Sulaiman GM. Potentials of iron oxide nanoparticles (Fe_3O_4): as antioxidant and alternative therapeutic agent against common multidrug-resistant microbial species potentials of iron oxide nanoparticles (Fe_3O_4): as antioxidant and alternative therapeutic agent against common multidrug-resistant microbial species. *Iraqi J Sci*. 2023;64(6):2759–2773.
10. Rukhsar M, Ahmad Z, Rauf A, et al. An overview of iron oxide (Fe_3O_4) nanoparticles: from synthetic strategies, characterization to antibacterial and anticancer applications. *Crystals*. 2022;12(12):1809. doi:10.3390/cryst12121809
11. Gupta V, Mohapatra S, Mishra H, et al. Nanotechnology in cosmetics and cosmeceuticals—a review of latest advancements. *Gels*. 2022;8(3):173. doi:10.3390/gels8030173
12. Tiwari N, Osorio-Blanco ER, Sonzogni A, et al. Nanocarriers for skin applications: where do we stand*? Angew Chem Int Ed*. 2022;61(3): e202107960. doi:10.1002/anie.202107960
13. Fytianos G, Rahdar A, Kyzas GZ. Nanomaterials in cosmetics: recent updates. *Nanomaterials*. 2020;10(5):979. doi:10.3390/nano10050979
14. Ganapathe LS, Mohamed MA, Mohamad yunus R, et al. Magnetite (Fe_3O_4) nanoparticles in biomedical application: from synthesis to surface functionalisation. *Magnetochemistry*. 2020;6(4):68. doi:10.3390/magnetochemistry6040068
15. Zhu G, Yu X, Xie F, et al. Ultraviolet light assisted heterogeneous Fenton degradation of tetracycline based on polyhedral Fe3O4 nanoparticles with exposed high-energy {110} facets. *Appl Surf Sci*. 2019;485:496–505. doi:10.1016/j.apsusc.2019.04.239
16. Gupta H, Kumar R, Park HS, et al. Photocatalytic efficiency of iron oxide nanoparticles for the degradation of priority pollutant anthracene. *Geosystem Eng*. 2017;20(1):21–27. doi:10.1080/12269328.2016.1218302
17. Ma S, Zhan S, Jia Y, et al. Superior antibacterial activity of Fe_3O_4 -TiO_2 nanosheets under solar light. *ACS Appl Mater Interfaces*. 2015;7 (39):21875–21883. doi:10.1021/acsami.5b06264
18. Zhang LY, Zhu XJ, Sun HW, et al. Control synthesis of magnetic Fe3O4–chitosan nanoparticles under UV irradiation in aqueous system. *Curr Appl Phys*. 2010;10(3):828–833. doi:10.1016/j.cap.2009.10.002
19. Nnorom IC, Igwe JC, Oji-Nnorom CG. Trace metal contents of facial (make-up) cosmetics commonly used in Nigeria. *Afr J Biotechnol*. 2005;4 (10):1133–1138.
20. Anghel I, Grumezescu AM, Andronescu E, et al. Magnetite nanoparticles for functionalized textile dressing to prevent fungal biofilms development. *Nanoscale Res Lett*. 2012;7(1):2–7. doi:10.1186/1556-276X-7-501
21. Huzaira M, Anderson RR. Magnetite tattoos. *Lasers Surg Med*. 2002;31(2):121–128. doi:10.1002/lsm.10075
22. Bystrzejewska-Piotrowska G, Golimowski J, Urban PL. Nanoparticles: their potential toxicity, waste and environmental management. *Waste Manag*. 2009;29(9):2587–2595. doi:10.1016/j.wasman.2009.04.001
23. Young AR, Claveau J, Rossi AB. Ultraviolet radiation and the skin: photobiology and sunscreen photoprotection. *JAAD*. 2017;76(3):S100–9. doi:10.1016/j.jaad.2016.09.038
24. Gromkowska-Kępka KJ, Puścion-Jakubik A, Markiewicz-żukowska R, Socha K. The impact of ultraviolet radiation on skin photoaging—review of in vitro studies. *J Cosmet Dermatol*. 2021;20(11):3427–3431. doi:10.1111/jocd.14033
25. Piluk TD, Faccio G, Letsiou S, et al. A critical review investigating the use of nanoparticles in cosmetic skin products. *Environ Sci Nano*. 2024;11 (3674):3674–3692. doi:10.1039/D4EN00489B
26. Netzlaff F, Lehr CM, Wertz PW, et al. The human epidermis models EpiSkin®, SkinEthic® and EpiDerm®: an evaluation of morphology and their suitability for testing phototoxicity, irritancy, corrosivity, and substance transport. *Eur J Pharm Biopharm*. 2005;60(2):167–178. doi:10.1016/j.ejpb.2005.03.004
27. Onoue S, Suzuki G, Kato M, et al. Non-animal photosafety assessment approaches for cosmetics based on the photochemical and photobiochemical properties. *Toxicol Vitr*. 2013;27(8):2316–2324. doi:10.1016/j.tiv.2013.10.003
28. Pellevoisin C, Bouez C, Cotovio J. Cosmetic industry requirements regarding skin models for cosmetic testing. In: *Skin Tissue Models*. Academic Press; 2018:3–37.
29. Kandárová H, Letaáiová S. Alternative methods in toxicology: pre-validated and validated methods. *Interdiscip Toxicol*. 2011;4(3):107–113. doi:10.2478/v10102-011-0018-6
30. Kandarova H, Liebsch M. The EpiDerm™ phototoxicity test (EpiDerm™ H3D-PT). *Alternatives Dermal Toxicity Testing*. 2017;483–503.
31. Ianoş R, Tăculescu A, Păcurariu C, et al. Solution combustion synthesis and characterization of magnetite, Fe_3O_4, nanopowders. *J Am Ceram Soc*. 2012;95(2236):2236–2240. doi:10.1111/j.1551-2916.2012.05159.x
32. Moaca EA, Farcaş C, Coricovac D, et al. Oleic acid double coated Fe3O4 nanoparticles as anti-melanoma compounds with a complex mechanism of activity-in vitro and in ovo assessment. *J Biomed Nanotechnol*. 2019;15(5):893–909. doi:10.1166/jbn.2019.2726
33. Moacă EA, Watz CG, Socoliuc V, et al. Biocompatible magnetic colloidal suspension used as a tool for localized hyperthermia in human breast adenocarcinoma cells: physicochemical analysis and complex in vitro biological profile. *Nanomaterials*. 2021;11(5):1189. doi:10.3390/nano11051189
34. Han CY, Lim SC, Choi HS, et al. Induction of ErbB2 by ultraviolet A irradiation: potential role in malignant transformation of keratinocytes. *Cancer Sci*. 2008;99(3):502–509. doi:10.1111/j.1349-7006.2007.00718.x
35. Kandarova H, Willoughby JA, De Jong WH, et al. Pre-validation of an in vitro skin irritation test for medical devices using the reconstructed human tissue model EpiDerm™. *Toxicol Vitr*. 2018;50(2017):407–417. doi:10.1016/j.tiv.2018.02.007
36. Moacă E, Watz CG, Ionescu DF, et al. Biosynthesis of iron oxide nanoparticles: physico-chemical characterization and their in vitro cytotoxicity on healthy and tumorigenic cell lines. *Nanomaterials*. 2022;12(12):2012. doi:10.3390/nano12122012
37. Zambzickaite G, Talaikis M, Dobilas J, et al. Microwave-assisted solvothermal synthesis of nanocrystallite-derived magnetite spheres. *Materials*. 2022;15(11):4008. doi:10.3390/ma15114008
38. Feld A, Weimer A, Kornowski A, et al. Chemistry of shape-controlled iron oxide nanocrystal formation. *ACS nano*. 2018;13(1):152–162. doi:10.1021/acsnano.8b05032

39. Manukyan K, Chen Y, Rouvimov S, et al. Ultrasmall α-Fe_2O_3 superparamagnetic nanoparticles with high magnetization prepared by template-assisted combustion process. *J Phys Chem C*. 2014;118(29):16264–16271. doi:10.1021/jp504733r
40. Unni M, Uhl A, Savliwala S, et al. Thermal decomposition synthesis of iron oxide nanoparticles with diminished magnetic dead layer by controlled addition of oxygen. *ACS Nano*. 2017;11(2):2284–2303. doi:10.1021/acsnano.7b00609
41. Kirkpatrick K, Zhou B, Bunting P, et al. Size-tunable magnetite nanoparticles from well-defined iron oleate precursors. *Chem Mater*. 2022;34 (17):8043–8053. doi:10.1021/acs.chemmater.2c02046
42. Frikha K, Bennici S, Bouaziz J, et al. Influence of the fuel/oxidant ratio on the elaboration of binary oxide catalyst by a microwave-assisted solution combustion method. *Energies*. 2020;13(12):3126. doi:10.3390/en13123126
43. Jordanova N, Jordanova D, Kostadinova-Avramova M, et al. A mineral magnetic approach to determine paleo-firing temperatures in the neolithic settlement site of Mursalevo-Deveboaz (SW Bulgaria). *J Geophys Res Solid Earth*. 2018;123(4):2522–2538. doi:10.1002/2017JB015190
44. Jin S, Shen P, Zhou D, et al. A common regularity of stoichiometry-induced morphology evolution of transition metal carbides, nitrides, and diborides during self-propagating high-temperature synthesis. *Cryst Growth Des*. 2012;12(6):2814–2824. doi:10.1021/cg201604z
45. Yang YF, Wang HY, Zhang J, et al. Lattice parameter and stoichiometry of TiCx produced in the Ti–C and Ni–Ti–C systems by self-propagating high-temperature synthesis. *J Am Ceram Soc*. 2008;91(8):2736–2739. doi:10.1111/j.1551-2916.2008.02486.x
46. Zou B, Jin S, Shen P, Jiang Q. Effect of reactant C/Ti ratio on the stoichiometry of Combustion-synthesized TiCx in Ti-C system. *JCS-Japan*. 2009;117(1364):525–528.
47. Yeh CL, Chen KT, Shieh TH. Effects of Fe/Si stoichiometry on formation of Fe3Si/FeSi-Al2O3 composites by aluminothermic combustion synthesis. *Metals*. 2021;11(11):1709. doi:10.3390/met11111709
48. Yun H, Liu X, Paik T, et al. Size-and composition-dependent radio frequency magnetic permeability of iron oxide nanocrystals. *ACS Nano*. 2014;8 (12):12323–12337. doi:10.1021/nn504711g
49. Salvioni L, Morelli L, Ochoa E, et al. The emerging role of nanotechnology in skincare. *Adv Colloid Interface Sci*. 2021;293:102437. doi:10.1016/j.cis.2021.102437
50. Nie J, Gao Q, Fu J, et al. Grafting of 3D bioprinting to in vitro drug screening: a review. *Adv Healthc Mater*. 2020;9(7):1901773. doi:10.1002/adhm.201901773
51. Masri S, Fauzi MB, Rajab NF, et al. In vitro 3D skin culture and its sustainability in toxicology: a narrative review. Artif Cells, Nanomedicine, Biotechnol. *Cells Nanomed Biotechnol*. 2024;52(1):476–499. doi:10.1080/21691401.2024.2407617
52. Kapałczyńska M, Kolenda T, Przybyła W, et al. 2D and 3D cell cultures – a comparison of different types of cancer cell cultures. *AMS*. 2018;14 (4):910–919. doi:10.5114/aoms.2016.63743
53. Choi J, Lee EJ, Jang WB, Kwon S-M. Development of biocompatible 3D-printed artificial blood vessels through multidimensional approaches. *J Funct Biomater*. 2023;14(10):497. doi:10.3390/jfb14100497
54. Pinzaru I, Tanase A, Enatescu V, et al. Proniosomal gel for topical delivery of rutin: preparation, physicochemical characterization and in vitro toxicological profile using 3D reconstructed human epidermis tissue and 2D cells. *Antioxidants*. 2021;10(1):85. doi:10.3390/antiox10010085
55. Chen L, Wu M, Jiang S, et al. Skin toxicity assessment of silver nanoparticles in a 3D epidermal model compared to 2D keratinocytes. *Int J Nanomed*. 2019;14:9707–9719. doi:10.2147/IJN.S225451
56. Kim H, Choi J, Lee H, et al. Skin corrosion and irritation test of nanoparticles using reconstructed three-dimensional human skin model, EpiDermTM. *Toxicol Res*. 2016;32(4):311–316. doi:10.5487/TR.2016.32.4.311
57. De Simone U, Spinillo A, Caloni F, et al. In vitro evaluation of magnetite nanoparticles in human mesenchymal stem cells: comparison of different cytotoxicity assays. *Toxicol Mech Methods*. 2020;30(1):48–59. doi:10.1080/15376516.2019.1650151
58. Foglia S, Ledda M, Fioretti D, et al. In vitro biocompatibility study of sub-5 nm silica-coated magnetic iron oxide fluorescent nanoparticles for potential biomedical application. *Sci Rep*. 2017;7(1):46513. doi:10.1038/srep46513
59. Asab G, Zereffa EA, Abdo Seghne T. Synthesis of Silica-Coated Fe3O4 nanoparticles by microemulsion method: characterization and evaluation of antimicrobial activity. *Int J Biomater*. 2020;2020(1):4783612. doi:10.1155/2020/4783612
60. Lourenço IM, Pelegrino MT, Pieretti JC, Andrade GP, Cerchiaro G, Seabra AB. Synthesis, characterization and cytotoxicity of chitosan-coated Fe3O4 nanoparticles functionalized with ascorbic acid for biomedical applications. In Journal of Physics: Conference Series (Vol. 1323, No. 1, p. 012015). 2019. IOP Publishing.
61. Tăculescu Moacă E, Coricovac D, Soica C, Pinzaru I, Păcurariu C, Dehelean C. Preclinical aspects on magnetic iron oxide nanoparticles and their interventions as anticancer agents: enucleation, apoptosis and other mechanism. In: Galvan RF, Barranco V, Galvan JC, Batlle SF, Fajardo S G, editors. *Iron Ores and Iron Oxide Materials*. IntechOpen; 2018:229–254.
62. Farcas CG, Dehelean C, Pinzaru IA, et al. Thermosensitive betulinic acid-loaded magnetoliposomes: a promising antitumor potential for highly aggressive human breast adenocarcinoma cells under hyperthermic conditions. *Int J Nanomed*. 2020;15:8175–8200. doi:10.2147/IJN.S269630
63. Farcas CG, Moaca EA, Dragoi R, et al. Preliminary results of betulinic acid-loaded magnetoliposomes - A potential approach to increase therapeutic efficacy in melanoma. *Rev Chim*. 2019;70(9):3372–3377. doi:10.37358/RC.19.9.7552
64. Prodan-Bărbulescu C, Watz CG, Moacă EA, et al. A preliminary report regarding the morphological changes of nano-enabled pharmaceutical formulation on human lung carcinoma monolayer and 3D bronchial microtissue. *Medicina*. 2024;60(2):208. doi:10.3390/medicina60020208
65. Lombrea A, Watz CG, Bora L, et al. Enhanced cytotoxicity and antimelanoma activity of novel semisynthetic derivatives of betulinic acid with indole conjugation. *Plants*. 2023;13(1):36. doi:10.3390/plants13010036
66. Zhao F, Zhao Y, Liu Y, et al. Cellular uptake, intracellular trafficking, and cytotoxicity of nanomaterials. *Small*. 2011;7(10):1322–1337. doi:10.1002/smll.201100001
67. Mahmoudi M, Azadmanesh K, Shokrgozar MA, et al. Effect of nanoparticles on the cell life cycle. *Chem Rev*. 2011;111(5):3407–3432. doi:10.1021/cr1003166
68. Balas M, Dumitrache F, Badea MA, et al. Coating dependent in vitro biocompatibility of new Fe-Si nanoparticles. *Nanomaterials*. 2018;8(7):1–26. doi:10.3390/nano8070495
69. Aits S, Jäättelä M, Nylandsted J. Methods for the quantification of lysosomal membrane permeabilization: a hallmark of lysosomal cell death. In: *Methods in Cell Biology*. Vol. 126. Academic Press; 2015:261–285.
70. Fan J, Dong H, Hu M, et al. Fluorescence imaging lysosomal changes during cell division and apoptosis observed using Nile Blue based near-infrared emission. *Chem Commun*. 2013;50(7):882–884. doi:10.1039/C3CC48043G

71. Bernstein EF, Sarkas HW, Boland P. Iron oxides in novel skin care formulations attenuate blue light for enhanced protection against skin damage. *J Cosmet Dermatol*. 2021;20(2):532–537. doi:10.1111/jocd.13803
72. Elbrolesy A, Abdou FAEY, Morsy R, Morsy R. Facile synthesis and biophysical characterization of Novel Zinc Oxide / Fe_3O_4 hybrid nanocomposite as a potentially active agent in sunscreens. *Arab J Sci Eng*. 2024;49(1):1083–1093. doi:10.1007/s13369-023-08082-3
73. Alili L, Chapiro S, Marten GU, et al. Effect of Fe_3O_4 nanoparticles on skin tumor cells and dermal fibroblasts. *BioMed Res Int*. 2015;2015 (1):530957. doi:10.1155/2015/530957
74. Caizer-Gaitan IS, Watz CG, Caizer C, et al. In vitro superparamagnetic hyperthermia employing magnetite gamma-cyclodextrin nanobioconjugates for human squamous skin carcinoma therapy. *Int J mol Sci*. 2024;25(15):8380. doi:10.3390/ijms25158380
75. Caizer C, Caizer IS, Racoviceanu R, et al. Fe3O4-PAA–(HP-γ-CDs) biocompatible ferrimagnetic nanoparticles for increasing the efficacy in superparamagnetic hyperthermia. *Nanomaterials*. 2022;12(15):2577. doi:10.3390/nano12152577